Article

Not peer-reviewed version

The Evolution of Dilatant Shear Bands in High Pressure Die Casting for Al-Si Alloy

JINGZHOU LU , ewan lordan , Kun Dou *

Posted Date: 2 October 2024

doi: 10.20944/preprints202410.0105.v1

Keywords: Shear bands; Segregation; Defects; Aluminium alloys; High pressure die casting

Article

The Evolution of Dilatant Shear Bands in High Pressure Die Casting for Al-Si Alloy

Jingzhou Lu [1], Ewan Lordan [2], Yijie Zhang [2], Zhongyun Fan [2], Wanlin Wang [1] and Kun Dou [1,*]

[1] School of Metallurgy and Environment, Central South University, Changsha, 410083, Hunan, China
[2] Brunel Centre for Advanced Solidification Technology (BCAST), Brunel University London, Kingston Lane, Uxbridge, UB8 3PH, United Kingdom
* Correspondence: Kun.Dou@csu.edu.cn; Tel.: +86 17600802394

Abstract: Bands of interdendritic porosity and positive macrosegregation are commonly observed in pressure die castings, with previous studies demonstrating their close relation to dilatant shear bands in granular materials. Despite recent technological developments, the micromechanism governing dilatancy in the high pressure die casting (HPDC) process for alloys between liquidus and solidus temperature region is still not fully understood. To investigate the influence of fluid flow and the size of externally solidified crystals (ESCs) on the evolution of dilatant shear bands in HPDC, various filling velocities were trialled to produce HPDC samples of Al8SiMnMg alloy. This study demonstrates that crystal fragmentation is accompanied by a decrease in dilatational concentration, thus producing an indistinct shear band. Once crystal fragmentation stagnates, the enhanced deformation rate associated with a further increase in filling velocity (from 2.2 ms^{-1} to 4.6 ms^{-1}) localises dilatancy into a highly concentrated shear band. The optimal piston velocity is 3.6 ms-1, under which the average ESC size reaches the minimum and the average yield stress and overall product of strength and elongation reaches the maximum value of 144.6 MPa and 3.664 GPa%, respectively. By adopting the concept of force chain buckling in granular media, the evolution of dilatant shear bands in equiaxed solidifying alloys can be adequately explained based on further verification with DEM-type modelling in OpenFOAM. Three mechanisms for ESC enhanced dilation are presented, elucidating previous reports relating the presence of ESCs to the subsequent shear band characteristics. By applying the physics of granular materials to equiaxed solidifying alloys, unique opportunities are presented for process optimization and microstructural modelling in HPDC.

Keywords: shear bands; segregation; defects; aluminium alloys; high pressure die casting

1. Introduction

High pressure die casting is a popular manufacturing processes for light metals and is known for high productivity, high dimensional accuracy and excellent mechanical properties. However, fierce turbulence occurs during the injection phase due to the rapid filling speed and narrow in-gate of the casting system. The J factor [Eq.1], which indicates the initial flow regime during filling, has received considerable attention in Japan, with recent studies aiming to establish the relation between its value and the subsequent product quality [1–3]. The J factor can be calculated using the VanRens equation:

$$J = D \cdot \rho \cdot V_g^{1.71} \quad [1]$$

Where V_g is the gate velocity, $D = ab/(a+b)$ is the orifice radius, a is the gate width, b is the gate thickness and ρ is the density of the alloy [3]. By capturing the high speed ejection of molten metal into an open space whilst irradiating laser light, Koya et al. demonstrate that flow becomes partially atomized at the time of injection given a sufficiently high J factor [4]. Atomization was attributed to two phenomena; (i) the collision of newly accelerated high speed material and previously injected low speed material, causing the front of the liquid jet to open like an umbrella, producing molten metal

 doi:10.20944/preprints202410.0105.v1

droplets with equivalent size range of the sauter mean diameter from its perimeter, and (ii) surface fluctuations of the liquid jet, which cause droplets of molten metal to separate from the liquid column [4,5], all of which occurs instantly before the melt temperature drops obviously, which can be treated as an isothermal process. Numerical modelling of the atomization phenomenon, achieved by a coupled large eddy simulation and volume of fluid approach, suggests that this atomized material is conveyed into the cavity as a multiphase flow containing finely dispersed air bubbles, persisting in this manner until filling is complete [5].

Intensive melt shearing, such as that introduced in the runner and ingate at the time of injection, has been shown to significantly influence the morphology and distribution of coarse externally solidified crystals (ESCs) observed in the final microstructure [6–10]. Wu et al. reported an increase in filling velocity led to the fragmentation and re-melting of crystals for an AM60B magnesium alloy, attributed to induced thermal shock and convection within the melt [9]. Li et al. discussed the rotation and fragmentation of crystals in relation to the aggregation of porosity within defect bands for an AZ91D magnesium alloy [10]. Gourlay et al. demonstrated that ESCs are not a prerequisite for the formation of defect bands, although their presence likely influence the rheology of the solidifying alloy, altering the characteristics of the residual band [11].

Previous studies on vane rheometry and direct shear cells have suggested that the rheology of equiaxed solidifying alloys can be interpreted as cohesionless compacted granular materials [12,13]. The grains within a compacted granular assembly respond to compressive and shear loading by rearranging to form regions of localised contraction and dilation. In equiaxed solidifying alloys such as Al-7Si-0.3Mg and Mg-9Al-0.7Z, an increase in shear stress is accompanied by a volumetric expansion (Reynold's dilatancy) [14]. As the shear stress increases, dilatancy develops in a highly anisotropic manner, ultimately localising within a narrow band following the casting contour. The thickness of shear bands commonly observed in HPDC components have been found to be in the range of 7-18 mean grains wide, within the characteristic range of 6-20 mean grains wide for dilatant shear bands in granular mediums [15]. The low crystal packing density of the band is expected to result in positive macrosegregation provided sufficient liquid can be drawn to the dilating band. When insufficient liquid is available, interdendritic porosity follows [14]. Previous studies have suggested that the HPDC process parameters influence the formation and characteristics of shear bands, with a key focus on controlling the intensification stage and the thermal conditions in the shot sleeve; however few have pondered the influence of flow conditions on the band characteristics [8,12,16,17].

Tordesillas characterises the evolution of stress-dilatancy within a cohesionless granular assembly via discrete element simulation (DEM), demonstrating that the underlying mechanism is one of cyclic jamming-unjamming events governed by the collective buckling of so-called force chains (self-organization of particles into load-bearing columnar structures, which align to the major principle stress axis prior to collapse) [18,19]. In this paper, we introduce the implications of force chain buckling on dilatant shear banding in equiaxed solidifying alloys, presenting three novel mechanisms for ESC enhanced dilation in HPDC. The influence of several filling velocities on the evolution of dilatant shear bands in HPDC will be discussed in relation to the initial jet flow conditions and the subsequent crystal morphology.

2. Materials and Method

2.1. Materials

35 Kg of Al8SiMnMg alloy (liquidus temperature of 615°C) with measured composition 8.1 wt. % Si, 0.44 wt. % Mn, 0.33 wt. % Mg, 0.06 wt. % Fe, 0.10 wt. % Ti and 0.02 wt. % Sr, was melted in an electric resistance furnace and then held at 750 °C for 30 min to maintain homogenization. The melt was degassed using a conventional rotary degassing unit for 10 min with a stirring speed of 350 rpm and an argon flow rate of 4 l/min.

2.2. Casting Technologies and Parameters

 doi:10.20944/preprints202410.0105.v1

During HPDC, molten metal was manually poured into the shot sleeve of a Frech 4500 kN locking force cold chamber HPDC machine using a transfer ladle. The temperature of the melt , the shot sleeve and the die cavity were maintained at 680 °C, 180 °C and 150 °C respectively. The molten metal was then injected into the die cavity with filling velocities of 2.2 ms^{-1}, 3.6 ms^{-1} and 4.2 ms^{-1} producing eight round tensile samples with nominal gauge diameter ø6.35 mm, in accordance with ASTM standards. Once the cavity was completely filled, an intensification pressure of 60 MPa was applied. A detailed description of the die geometry used to produce these tensile specimens can be found in [20] and is shown in Figure 1, and the piston profiles used in this work is shown in Figure 2. The entire piston stroke is 470 mm, during the initial shot stages in three velocity profiles, the piston velocity increases from 0 to 0.4 ms^{-1} and then gradually to 0.6 ms^{-1}. During the fast shot stage, the three velocity profiles differ in filling speed as mentioned above. The reason for selection of characteristic filling velocities of 2.2 ms^{-1}, 3.6 ms^{-1} and 4.2 ms^{-1} are described in detail in previous works of the authors[31,32].

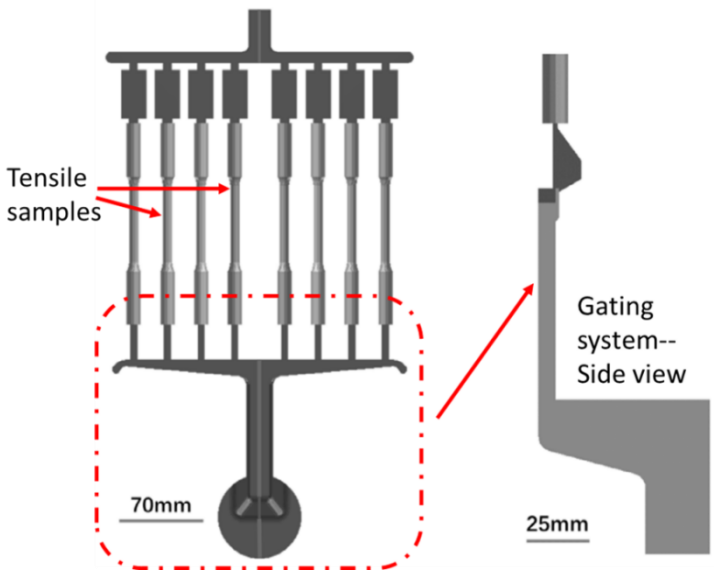

Figure 1. Casting region with gating system and 8 tensile samples HPDC tensile.

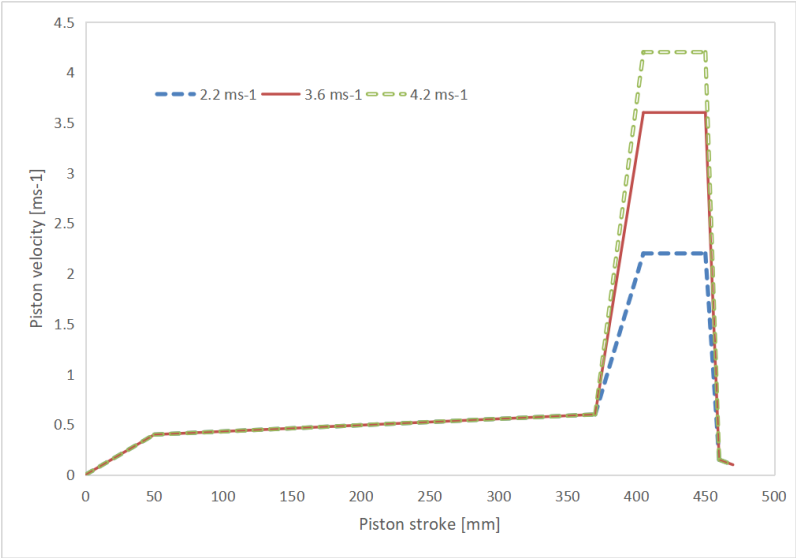

Figure 2. Shot profile highlighting filling velocities used to produce HPDC tensile specimens.

To ensure a steady-state die temperature, a FLIR T650sc infrared camera was used to capture thermographic data. From the infrared images, temperature readings were taken from the centre of

 doi:10.20944/preprints202410.0105.v1

the gage section and at the ingate using point measurements within the thermographic post-processing software FLIR tools (version FLIR Tools+ 6.4.18039.1003). An illustration of the infrared image and the temperature readings are shown in Figure 3. It was found that after six shots, a steady state die temperature was achieved. The first six shots were therefore scrapped, and samples were taken from proceeding shots.

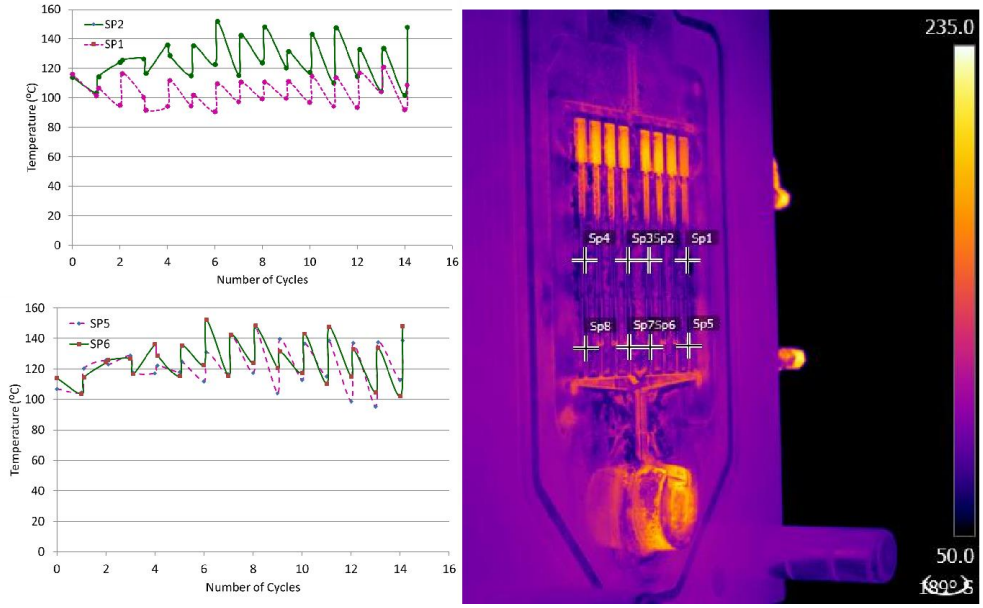

Figure 3. Infrared image and the temperature readings during various cycles of the HPDC process.

2.3. Tensile Test

Tensile tests were performed at ambient temperature using an Instron 5500 universal electromechanical testing system, in accordance with ASTM standard E8/E8M . The gauge length and gauge diameter of the tensile specimens are 55 mm and 6.35 mm, respectively. Tensile data was recorded using a 50 mm extensometer with a ramp rate of 1 mm/min.

2.4. Microstructure Characterization

Samples for microstructural observation were taken from the centre of the gauge length, acting perpendicular to the tensile direction. Samples were ground and polished to a 1 μm finish using standard metallographic techniques. To reveal the microstructure samples were etched with Keller's reagent (95% H_2O, 2.5% HNO_3, 1.5% HCl, and 1% HF). Optical microscopy and scanning electron microscopy (SEM) were used to observe the etched microstructures of the HPDC samples. High contrast SEM micrographs for grain size measurements were obtained via a tungsten filament Carl Zeiss LEO 1455VP SEM and analyzed using the Fiji image processing software package based on ImageJ.

3. Results

3.1. Dilatant Shear Bands and ESC Morphology

Bands of positive macrosegregation were observed with all filling velocities trialled in this study (Figure 4). With an increase in velocity from 2.2 ms^{-1} to 3.6 ms^{-1}, dilatational concentration (defined here as the degree of local dilation, thus characterized by the local eutectic fraction) was observed to decrease, suggesting a transition from localised dilation within a shear band to global dilation of the entire assembly. Further increasing the filling velocity from 3.6 ms^{-1} to 4.2 ms^{-1} once again produced a distinct shear band. The normalized width of the Si enrichment region in figure 3 (red dash line area) are estimated in ImageJ software and the normalized values are 0.92, 0.52 and 0.85 respectively when filling speed increases from 2.2 ms^{-1} to 4.2 ms^{-1}.

 doi:10.20944/preprints202410.0105.v1

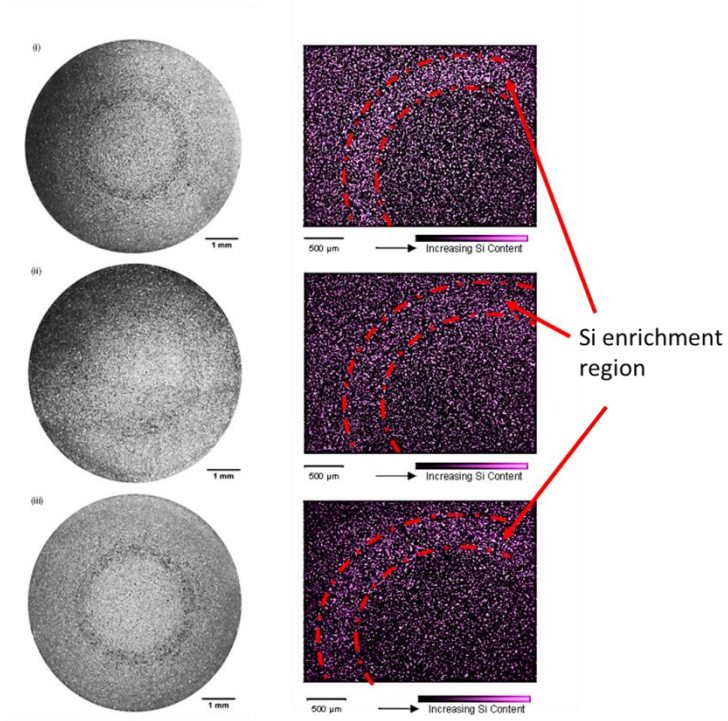

Figure 4. Dilatant shear bands observed in HPDC samples produced with filling velocities of 2.2 ms^{-1} (top row), 3.6 ms^{-1} (middle row) and 4.2 ms^{-1} (bottom row). Typical macrostructure of etched samples from the centre of the gage section are shown (left) and corresponding EDX maps highlighting eutectic fraction are shown (right).

For samples produced with filling velocities of 2.2 ms^{-1} and 4.2 ms^{-1}, large fluctuations in eutectic fraction were observed within the band, reminiscent of the large voids attributed to force chain buckling in granular media (Figure 5). Outlined in Figure 5 ii is a columnar crystal structure residing in the shear band of a sample produced at 3.6 ms^{-1}, observed to offset slightly from the major principle stress axis (i.e. radial compression during intensification)

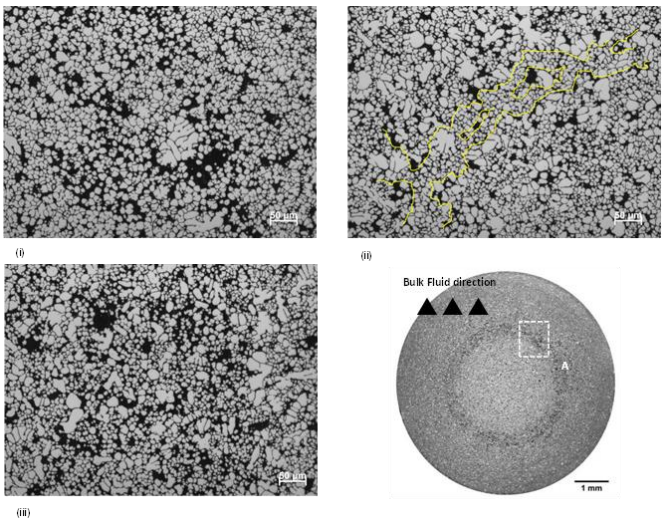

Figure 5. Optical micrographs taken from zone A, showing how dilatancy varies with filling velocities of (i) 2.2 ms^{-1}, (ii) 3.6 ms^{-1}, and (iii) 4.2 ms^{-1}. Outlined in (ii) is a potential force chain that has persisted through deformation. The bulk filling direction is out of the page.

3.2. Grain Size and mechanical Properties

 doi:10.20944/preprints202410.0105.v1

High contrast SEM micrographs captured within the shear band were used to determine the average size of ESCs and in-cavity solidified grains for samples produced with the aforementioned filling velocities (Table 1). Within the Fiji image processing software package based on ImageJ, SEM micrographs were binarized using an appropriate threshold to differentiate grains from the matrix(Figure 6). The average grain size (Φ) was determined using the equivalent circle approach (Eq. 2). Grains with a diameter ≥ 20 μm were defined as ESCs and were separated from in-cavity solidified grains (3 μm ≤ ϕ_i ≤ 20 μm) for subsequent analysis.

$$Area\ of\ crystal = \pi\phi_i/4\,,\ \phi = \sum(\phi_i/N_p) \quad (2)$$

An increase in filling velocity from 2.2 ms^{-1} to 3.6 ms^{-1} resulted in a decrease in the average ESC size from 41 μm to 27 μm. A further increase in velocity from 3.6 ms^{-1} to 4.2 ms^{-1} did not significantly alter the average ESC size, with only slight increase from 27 μm to 33 μm, however, considerably reduced average size of in cavity solidified grains are observed in this process, with the mean values decreasing from 8.1 μm to 7.3 μm.

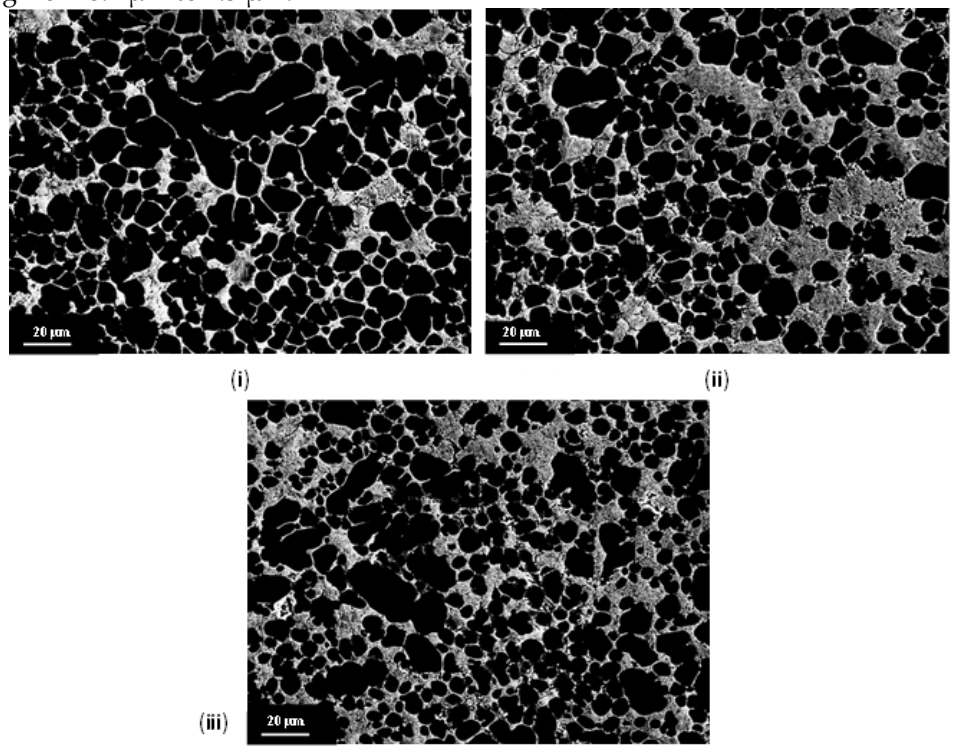

Figure 6. Typical high contrast secondary electron SEM micrographs used to obtain average ESC and in-cavity solidified grain size (Table.1), for filling velocities of (i) 2.2 ms^{-1}, (ii) 3.6 ms^{-1} and (iii) 4.2 ms^{-1}.

Table 1. Average ESC and in-cavity solidified grain sizes within the shear band. All values were calculated using the Fiji (ImageJ) software from high contrast secondary electron SEM micrographs such as those shown in Figure 4.

Filling Velocity (ms^{-1})	Average ESC Φ (μm)	Average in cavity grain Φ (μm)
2.2	41	8.1
3.6	27	8.1
4.2	33	7.3

The yield stress, elongation and ultimate tensile stress of various tensile samples are tested and plotted in Figure 7. As is shown in the figure, the mechanical properties shows some variability in different locations and under various piston speed. The average values for the mechanical properties are summarized in Table 2. Combining Table 1 and Table 2, it could be seen that with the piston velocity of 3.6ms-1, the average ESC size reaches the minimum and the average yield stress and

 doi:10.20944/preprints202410.0105.v1

overall product of strength and elongation reaches the maximum value of 144.6 MPa and 3.664 GPa%, respectively.

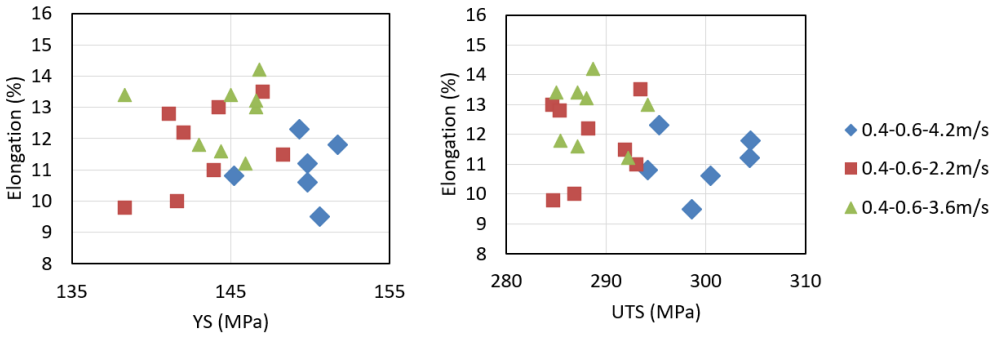

Figure 7. The yield stress, elongation and ultimate tensile stress of various tensile samples.

Table 2. Summary of mechanical properties under various piston velocities.

	Average			
Casting parameters	**YS (MPa)**	**UTS (MPa)**	**Elongation [%]**	**Product of strength and elongation (GPa%)**
0.4-0.6, 2.2m/s	143.0	288.5	11.5	3.318
0.4-0.6, 3.6m/s	144.6	288.5	12.7	3.664
0.4-0.6, 4.2m/s	143.7	292.8	11.3	3.309

4. Discussion

Within a compacted granular material, stress is heterogeneously transmitted along a two-phase network of contacts [18,21]. The "strong network" is defined as a subnetwork comprising chains of highly stressed particles, which carry the majority of the applied load. The complementary "weak network" consists of contacts that experience a below average force and provides lateral support to existing force chains. Whilst Radjai very appropriately states "the weak network behaves essentially as an interstitial liquid, whereas the strong forces carry the whole deviatoric load and in this respect behaves as a solid", we cannot simply reverse this analogy to describe microstructural evolution during equiaxed solidification without first considering that the weak network is more likely to compose a dilute suspension of liquid and dispersed crystals.

Initial deformation of the granular medium is predominately affine, with potential energy increasing with strain [18,19]. At the onset of non-affine deformation, force chains establish and align to the major principal stress axis. The absence of force chain buckling is accompanied by global dilation of the granular assembly [18,19,22]. Force chain buckling initiates just prior to peak shear stress, generating large voids between neighbouring columns [23–25]. After the peak shear stress, force chain buckling propagates causing dilatancy to localise within a narrow shear band [19]. When a force chain fails (unjamming event), the energy stored at its contacts is dissipated to neighbouring particles from the weak network, encouraging the formation of new force chains or the reinforcement of existing ones (jamming event) [19]. The shear band continues to develop, until these cyclic unjamming-jamming events cause the band to reach a residual state, in which the collapse of existing force chains is in equilibrium with the generation of new microstructure [24]; however, when deliberating dilatancy in equiaxed solidifying alloys, one must consider that with sufficiently high cooling rates, the casting may solidify before the band achieves this residual state.

Particle rotation during filling has been widely reported, predominantly originating from highly turbulent flow conditions and subsequent particle interactions within the multiphase suspension [10,26–29]. The size (10~200 μm) and morphology (globular/irregular) of these particles greatly influences the flow of the suspension. In a given velocity gradient, increasing the particle size leads to enhanced rotation and an increased collision frequency [26]. It is evident from (Figure 4, 5, Table.1)

 doi:10.20944/preprints202410.0105.v1

that crystal fragmentation is accompanied by a decrease in dilatational concentration, with normalized width of the Si enrichment region decreasing from 0.92 to 0.52. Surmising the concept of force chain buckling in equiaxed solidifying alloys, we can explain the influence of fluid flow and crystal morphology on dilatant shear banding in HPDC. Figure 8 illustrates three novel mechanisms of ESC enhanced dilation proposed by the authors:

(1) In Figure 8i, the presence of large crystals within the force chain leads to a decrease in the total number of contacts and increases the volume of interstitial fluid. The force chain is therefore more susceptible to buckling, enhancing dilation within the shear band.

(2) Particles within the shear band experience a transverse lift force, due to the existence of a non-uniform pressure distribution. This lift force encourages crystals to migrate towards the region of lowest shear stress [26] (i.e. the centreline of the band). An increase in particle size is accompanied by an increase in lift force. According to the lift force models in [32], an increase of particle size from 50 to 100 μm will lead to an incease of 2.5e-9 N in lift force. Within the band, ESCs that comprise the outermost regions of the force chain will effectively act as pivots (Figure 8ii), with the applied moment resulting from the aforementioned slip-shear lift forces.

(3) Within a given velocity gradient, increasing the particle size will increase the energy dissipated upon collision. In Figure 8iii, a large crystal travelling at high velocity may possess the potential to dislodge a segment of the force chain, provided the energy dissipated upon collision is sufficient to encourage local particle rearrangement. This phenomenon is likely to occur towards the centreline of the shear band where resistance to flow is at a minimum, and particle momentum is likely to be at a maximum.

With a further increase in filling velocity from 3.6 ms^{-1} to 4.2 ms^{-1}, the average size of ESCs was observed to remain relatively stable. This suggests that crystal fragmentation stagnates at a threshold J-factor, governed by the ingate geometry. For the ingate geometry used throughout this series of experiments, the filling velocity threshold corresponding to the atomization phenomenon is 0.71 ms^{-1}. Therefore it can be assumed that for all filling velocities trialled in this study, melt flowing into the die cavity consists of a liquid column, encompassing a large proportion of ESCs, and fine droplets that rapidly solidify due to their small volume.

Despite the apparent stability in the average ESC size, dilatancy was observed to once again localise into a distinct shear band for samples produced at 4.2 ms^{-1}. This is likely to result from the increased shear stress introduced at 4.2 ms^{-1}, increasing the rate of force chain buckling within the band. Considerable refinement of the in-cavity solidified grains from 8.1 μm to 7.3 μm was also observed following the increase in filling velocity from 3.6 ms^{-1} to 4.2 ms^{-1}. This was attributed to the atomization phenomenon, wherein an increase in injection velocity is accompanied by a reduction in droplet diameter [30].

 doi:10.20944/preprints202410.0105.v1

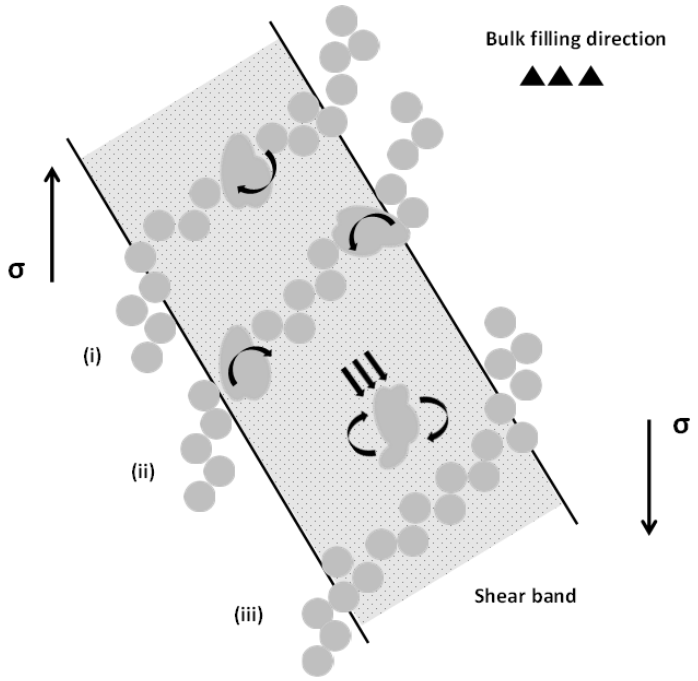

Figure 8. Graphical illustration highlighting the three mechanisms governing ESC enhanced dilation within the shear band: (i) 'Stacking faults' introduced by the presence of ESCs along the force chain; (ii) ESCs located on the outermost regions of the band effectively acting as pivots; (iii) ESCs propelled by highly turbulent flow conditions, potentially dislodging crystals from the force chain. σ denotes the major principle stress axis.

To further validate the above mechanism, the melt flow and ESC motion during the HPDC process are modeled based on OpenFOAM v5.0 platform. Considering similarity and to reduce the computation time of the entire fill system as is shown in Figure 1. A single tensile sample including its ingate and overflow is selected as the modelling region to obtained the characteristic fluid flow and ESC motion behavior. The melt flow behavior is modeled by solving the Navior-Stokes equations and Standard k-epsilon equations. The ESC motion is described using DPMFoam in OpenFOAM. The mesh is generated using blockMesh and snappyHexMesh. Considering the minimum length for the calculation domain is 2mm (ingate thickness direction), a mesh size of 0.5 mm is used for accurate description of the flow problem. The fluid velocity distribution and ESC motion velocity distribution are shown in Figure 9. It could be known that during the melt filling process, the ESCs tend to flow and aggregate towards the central region along the flow direction in the tensile sample. The ESCs aggregation tendency is described in Figure 10. The legend stands for the averaged number density in ESC particles in the different locations in a tensile sample. It could be clearly seen that this model could accurately predict the evolution of dilatant shear bands in compacted granular assemblies and further validate the proposed mechanism for evolution of dilatant shear bands in high pressure die casting for Al-Si alloy.

Preprints.org (www.preprints.org) | NOT PEER-REVIEWED | Posted: 2 October 2024 doi:10.20944/preprints202410.0105.v1

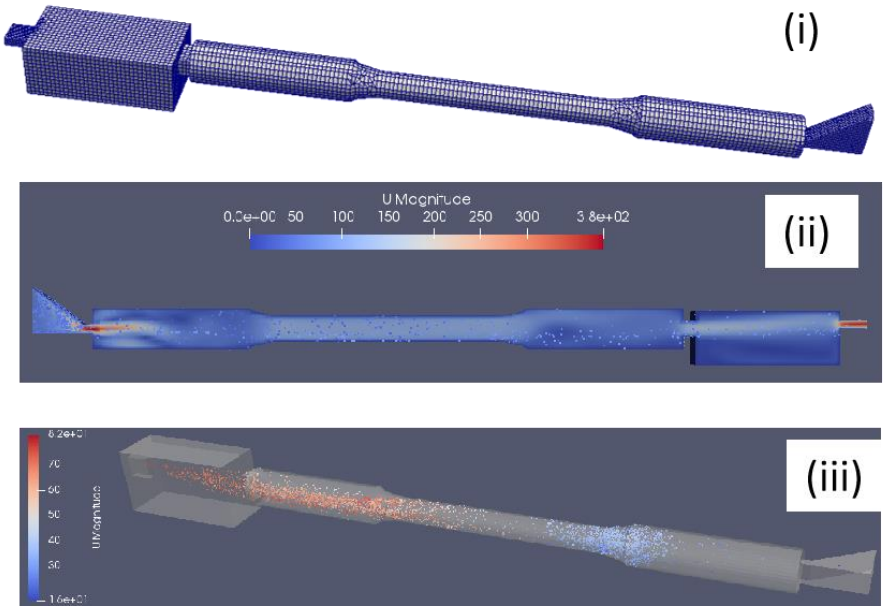

Figure 9. (i) Calculation domain and mesh for the model, (ii)The fluid velocity distribution of melt, (iii) The ESC motion and velocity distribution in the tensile sample during filling.

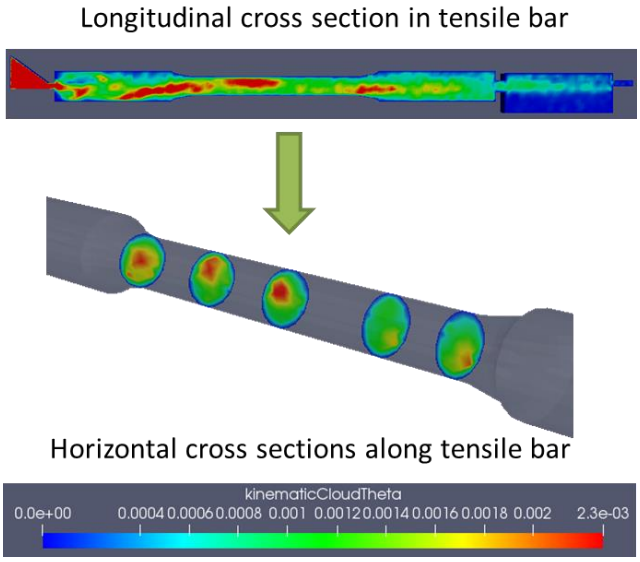

Figure 10. The ESCs aggregation tendency in the tensile sample during filling.

5. Conclusions

By adopting the concept of force chain buckling in compacted granular materials, the evolution of dilatant shear bands in equiaxed solidifying alloys can be adequately explained. Fluid flow and grain size were found to significantly influence dilatancy, governing dilatational concentration and subsequently the extent of segregation within the band. The maximum dilatancy of 0.92 (normalized width of the Si enrichment region) is observed when the flow filling speed is 2.2 ms^{-1} and the average ESC size is 41 μm. Increasing the filling velocity appeared to promote crystal fragmentation up until a critical J-factor, leading to a decrease in dilatational concentration and thus a less distinct shear band. Excessive filling velocities increased the deformation rate, leading to an increase in dilatational concentration, and a distinct shear band; however also led to considerable refinement of in-cavity solidified grains, attributed to the atomization phenomenon. To explain the influence of grain size

 doi:10.20944/preprints202410.0105.v1

and crystal morphology on the evolution of dilatant shear bands in HPDC, three novel mechanisms for ESC enhanced dilation are presented:

(1) 'Stacking faults' introduced by the presence of large crystals within the force chain reduce the total number of contacts and increase the volume of interstitial fluid, weakening the structure.

(2) Crystals located towards the outermost region of the band are drawn inwards by slip-shear lift forces. A force chain comprising large crystals at its pivots will experience a greater moment, increasing susceptibility to buckling.

(3) A larger crystal travelling at increasing piston velocity from 2.2 ms^{-1} to 4.2 ms^{-1} may possess the potential to dislodge a segment of a given force chain, provided the energy dissipated upon collision is sufficient to incite local particle rearrangements. The optimal piston velocity is 3.6 ms^{-1}, under which the average ESC size reaches the minimum and the average yield stress and overall product of strength and elongation reaches the maximum value of 144.6 MPa and 3.664 GPa%, respectively.

(4) Force chain buckling has been studied with sophisticated DEM-type simulations using OpenFOAM platform, which is able to accurately predict the evolution of dilatant shear bands in compacted granular assemblies. By applying the physics of granular materials to equiaxed solidifying alloys, unique opportunities are presented for process optimization and microstructure modelling once further testing of other alloys are conducted.

Author Contributions: Conceptualization, K. D.; methodology, K. D.; software, K. D.; validation, K. D., E. L. and Z. F.; formal analysis, Z. F.; investigation, J. L.; resources, K. D.; data curation, Y. Z.; writing—original draft preparation, J. L.; writing—review and editing, K. D.; visualization, J. L.; supervision, K. D., E. L. and Z. F.; W. W.; project administration, K. D.; funding acquisition, Z. F.; W. W. All authors have read and agreed to the published version of the manuscript.

Funding: This research was funded by the National Science Foundation of China (52304360) and the Open foundation of the State Key Laboratory of Advanced Metallurgy, University of Science and Technology Beijing, China (K22-07), the Key Research and Development Program of Xiangjiang Laboratory (22XJ01002) and Engineering and Physical Sciences Research Council (EPSRC) and Jaguar Land Rover Ltd. [grant number 11055100].

Informed Consent Statement: Informed consent was obtained from all subjects involved in the study.

Data Availability Statement: The original contributions presented in the study are included in the article/supplementary material, further inquiries can be directed to the corresponding author/s.

Acknowledgments: This work was supported by the National Science Foundation of China (52304360) and the Open foundation of the State Key Laboratory of Advanced Metallurgy, University of Science and Technology Beijing, China (K22-07), the Key Research and Development Program of Xiangjiang Laboratory (22XJ01002) and Engineering and Physical Sciences Research Council (EPSRC) and Jaguar Land Rover Ltd. [grant number 11055100].

Conflicts of Interest: The authors declare no conflicts of interest.

References

1. T. Kaneuchi, H. Nakano, Effect of J-value for internal quality of HPDC products at various casting alloys, in: Japan Die Cast. Congr. Trans., 2008: pp. 131–136.
2. T. Kaneuchi, K. Motegi, T. Imamura, Properties of castings produced by high vacuum die cast process, in: Japan Die Cast. Congr. Trans., 2004: pp. 277–282.
3. Y. Yamada, H. Yoshii, S. Mochizuki, Evaluation of J factor and leakage quality for high pressure die casting applied to closed-deck type cylinder block, SAE Tech. Pap. (2011).
4. E. Koya, M. Nakagawa, S. Kitagawa, J. Ishimoto, Y. Nakano, N. Ochiai, Research of Atomization Phenomena in HPDC-Step 1 Feature of Gas Porosity Dispersion and Photography of Atomized Flow, SAE Tech. Pap. 2018–April (2018) 1–8. doi:10.4271/2018-01-1392.
5. E. Koya, M. Nakagawa, S. Kitagawa, J. Ishimoto, Y. Nakano, N. Ochiai, Atomization in High-Pressure Die Casting - Step 2 Simulation of Atomized Flow of Molten Aluminum by LES-VOF Method, SAE Tech. Pap. 2018–April (2018) 1–10. doi:10.4271/2018-01-1393.

6. S. Otarawanna, C.M. Gourlay, H.I. Laukli, A.K. Dahle, Agglomeration and bending of equiaxed crystals during solidification of hypoeutectic Al and Mg alloys, Acta Mater. 58 (2010) 261–271. doi:10.1016/j.actamat.2009.09.002.
7. H.R. Kotadia, N. Hari Babu, H. Zhang, S. Arumuganathar, Z. Fan, Solidification behavior of intensively sheared hypoeutectic Al-Si alloy liquid, Metall. Mater. Trans. A Phys. Metall. Mater. Sci. 42 (2011) 1117–1126. doi:10.1007/s11661-010-0516-8.
8. H. Cao, M. Wessén, Characteristics of microstructure and banded defects in die cast AM50 magnesium components, Int. J. Cast Met. Res. 18 (2005) 377–384. doi:10.1179/136404605225023216.
9. M. Wu, X. Li, Z. Guo, S.Xiong, Effects of process parameters on morphology and distribution of externally solidified crystals in microstructure of magnesium alloy die castings, China Foundry. 15 (2018) 139–144. doi:10.1007/s41230-018-7242-z.
10. X. Li, Z. Guo, S. Xiong, Influence of melt flow on the formation of defect band in high pressre die casting of AZ91D magnesium alloy, Mater. Charact. 129 (2017) 344–352.
11. C.M. Gourlay, H.I. Laukli, A.K. Dahle, Defect band characteristics in Mg-Al and Al-Si high-pressure die castings, Metall. Mater. Trans. A Phys. Metall. Mater. Sci. 38 (2007) 1833–1844. doi:10.1007/s11661-007-9243-1.
12. A.K. Dahle, D.H. StJohn, Rheological behaviour of the mushy zone and its effect on the formation of casting defects during solidification, Acta Mater. 47 (1998) 31–41. doi:10.1016/S1359-6454(98)00342-5.
13. AZ91 magnesium alloy, Acta Mater. 56 (2008) 3403–3413. doi:10.1016/j.actamat.2008.03.020.
14. C.M. Gourlay, A.K. Dahle, Dilatant shear bands in solidifying metals, Nature. 445 (2007) 70–73. doi:10.1038/nature05426.
15. S. Otarawanna, C.M. Gourlay, H.I. Laukli, A.K. Dahle, The thickness of defect bands in high-pressure die castings, Mater. Charact. 60 (2009) 1432–1441. doi:10.1016/j.matchar.2009.06.016.
16. H. Gjestland, S. Sannes, J. Svalestuen, H. Westengen, Optimizing the Magnesium Die Casting Process to Achieve Reliability in Automotive applications, SAE Tech. Pap. Ser. SAE 2005-0 (2005). doi:10.4271/2005-01-0333.
17. S. Otarawanna, H.I. Laukli, C.M. Gourlay, A.K. Dahle, Feeding mechanisms in high-pressure die castings, Metall. Mater. Trans. A Phys. Metall. Mater. Sci. 41 (2010) 1836–1846. doi:10.1007/s11661-010-0222-6.
18. A. Tordesillas, J. Shi, T. Tshaikiwsky, Stress–dilatancy and force chain evolution, Int. J. Numer. Anal. Meth. Geomech. 35 (2011) 264–292.
19. A. Tordesillas, Force chain buckling, unjamming transitions and shear banding in dense granular assemblies, Philos. Mag. 87 (2007) 4987–5016. doi:10.1080/14786430701594848.
20. E. Lordan, J. Lazaro-Nebreda, Y. Zhang, Z. Fan, Effective Degassing for Reduced Variability in High-Pressure Die Casting Performance, JOM. (2018). doi:10.1007/s11837-018-3186-4.
21. F. Radjai, D. Wolf, M. Jean, J.J. Moreau, F. Radjai, D. Wolf, M. Jean, J. Jacques, M. Bimodal, Bimodal Character of Stress Transmission in Granular Packings To cite this version : HAL Id : hal-01407369 Bimodal Character of Stress Transmission in Granular Packings, (2016) 0–4.
22. D. walker, A. tordesillas, On Reynolds' Dilatancy and Shear Band Evolution: a New Perspective, Int. J. Bifurc. Chaos. 23 (2013) 1330034. doi:10.1142/S0218127413300346.
23. M. Oda, J. Konishi, S. Nemat-Nasser, Experimental micromechanical evaluation of the strength of granular materials: Effects of particle rolling, Stud. Appl. Mech. 7 (1983) 21–30. doi:10.1016/B978-0-444-42192-0.50009-8.
24. K. Iwashita, M. Oda, Micro-deformation mechanism of shear banding process based on modified distinct element method, Powder Technol. 109 (2000) 192–205. doi:10.1016/S0032-5910(99)00236-3.
25. T.S. Majmudar, R.P. Behringer, Contact force measurements and stress-induced anisotropy in granular materials, Nature. 435 (2005) 1079–1082. doi:10.1038/nature03805.
26. H.I. Laukli, C.M. Gourlay, A.K. Dahle, Migration of crystals during the filling of semi-solid castings, Metall. Mater. Trans. A Phys. Metall. Mater. Sci. 36 (2005) 805–818. doi:10.1007/s11661-005-1011-5.
27. H.I. Andersson, L. Zhao, M. Barri, Torque-coupling and particle-turbulence interactions, J. Fluid Mech. 696 (2012) 319–329. doi:10.1017/jfm.2012.44.
28. C. Bi, S. Xiong, X. Li, Z. Guo, Development of a Fluid-Particle Model in Simulating the Motion of External Solidified Crystals and the Evolution of Defect Bands in High-Pressure Die Casting, Metall. Mater. Trans. B Process Metall. Mater. Process. Sci. 47 (2016) 939–947. doi:10.1007/s11663-016-0591-3.

 doi:10.20944/preprints202410.0105.v1

29. X. Li, W. Yu, J. Wang, S. Xiong, Influence of melt flow in the gating system on microstructure and mechanical properties of high pressure die casting AZ91D magnesium alloy, Mater. Sci. Eng. A. 736 (2018) 219–227. doi:10.1016/j.msea.2018.08.090.
30. I. Graco, Atomization Concept and Theory, 1995.
31. K. Dou, E. Lordan, Y. Zhang, A. Jacot, Z. Fan. A complete computer aided engineering (CAE) modelling and optimization of high pressure die casting (HPDC) process. Journal of Manufacturing Processes, 2020. doi.org/10.1016/j.jmapro.2020.10.062.
32. K. Dou, E. Lordan, Y. Zhang, A. Jacot, Z. Fan. A novel approach to optimize mechanical properties for aluminium alloy in High pressure die casting (HPDC) process combining experiment and modelling. Journal of Materials Processing Technology, 2021. doi.org/10.1016/j.jmatprotec.2021.117193.
33. Bi, C., Xiong, S., Li, X. et al. Development of a Fluid-Particle Model in Simulating the Motion of External Solidified Crystals and the Evolution of Defect Bands in High-Pressure Die Casting. Metall Mater Trans B 47, 939–947 (2016). https://doi.org/10.1007/s11663-016-0591-3.